Mn_5Ge_3 film formation on Ge(111)$c(2 \times 8)$

J. Hirvonen Grytzelius,* H. M. Zhang, and L. S. O. Johansson
Department of Physics, Karlstad University, S-651 88 Karlstad, Sweden
(Received 28 May 2012; published 18 September 2012)

Thin manganese germanide films with different thicknesses on Ge(111) have been studied in detail by low-energy electron diffraction (LEED), scanning tunneling microscopy, and core-level spectroscopy (CLS). Annealing of the deposited Mn on Ge(111)$c(2 \times 8)$ between 330–450 °C resulted in well-ordered Mn_5Ge_3 surfaces as seen by intense $\sqrt{3} \times \sqrt{3}$ LEED spots. Up to a coverage of 24 monolayers (ML), island formation is favored. At a coverage of 32 ML, a well-ordered Mn_5Ge_3 film was found to fully cover the surface. High-resolution Ge 3*d* CLS spectra were recorded with photon energies between 50 and 110 eV at normal and 60° emission angles. In contrast to earlier results, three components have been used in the line-shape analysis to achieve a consistent fit over the energy and angular range. In addition, three components have been identified for the Mn 2*p* CLS spectra. The two major components fit well with a layered Mn germanide structure suggested in the literature.

DOI: 10.1103/PhysRevB.86.125313 PACS number(s): 68.37.Ef, 68.35.bg, 68.35.Fx

I. INTRODUCTION

Magnetic materials based on Mn and Ge have received a lot of attention lately. There are two important facts that make the MnGe alloy interesting. First, Mn germanides show magnetic properties at a temperature of ∼300 K.[1,2] Second, germanium-based alloys are relatively easy to integrate into today's existing silicon-based technology. Thus, these materials are expected to be good candidates for spintronics applications.[3] However, despite many theoretical and experimental efforts, it is still not yet clear in many fundamental issues, such as growth mode and electronic structure that are related to the surface magnetic property.

Thin Mn_5Ge_3 films on Ge(111) grown by solid phase epitaxy have been studied by several groups.[1,4–6] Zeng *et al.*[1] reported that the annealing of the as-deposited manganese between 300–650 °C always results in uniform, ferromagnetic Mn_5Ge_3 films and that the ordered $\sqrt{3} \times \sqrt{3}$ surface reconstruction should be associated with the Mn_5Ge_3 phase. Sangaletti *et al.* and De Padova *et al.* provided further evidence for surface ferromagnetism in the Mn germanide film with a $\sqrt{3} \times \sqrt{3}$ surface reconstruction.[6,7] The low-coverage regime has also been particularly investigated in several studies.[4,8,9] Annealing of the as-deposited manganese at 400 °C results in a seed layer for further growth of Mn_5Ge_3.[4] Scanning tunneling microscopy (STM) studies, on the other hand, have shown that all Mn germanide films grown by solid phase epitaxy on Ge(111) and Ge(100) have similar surface structures with the Mn_5Ge_3(0001) exposed plane.[3,4,10,11]

In this paper, we present our experimental results regarding the film morphology, and electronic properties of thin solid phase epitaxy grown Mn_5Ge_3 films with a Mn content from 6 to 32 monolayers (ML). The surfaces have been investigated in detail by low-energy electron diffraction (LEED), STM, and core-level spectroscopy (CLS). The film morphology at the different Mn coverages reveals a stacked film structure, in good agreement with earlier atomic models.[12,13] Three components have been found in the Ge 3*d* CLS spectra. For the Mn 2*p* core-level spectra, the surface component is shifted towards higher binding energy, which is opposite to the Ge case.

II. EXPERIMENTAL DETAILS

The STM study was performed in a variable temperature STM system from Omicron Nanotechnology GmbH. The STM tip was made from a W wire. All STM images in this paper were recorded in constant current mode. The CLS studies were performed at beamline (BL) 33/I4 and I311 at the MAX-lab synchrotron radiation facility in Lund, Sweden.[14] The Ge 3*d* core-level spectra were obtained with an energy resolution of ∼50 meV and an angular resolution of ±2° at BL 33/I4. The Mn core-level spectra were recorded in normal emission with an acceptance angle of about 15° at BL I311. The energy resolution was ∼200 meV for the Mn 2*p* spectra. Ge(111) samples were cut from commercially available *n*-doped single-crystal wafers (Sb, 3 Ω cm). The samples were outgassed *in situ* by direct current heating at 500 °C for several hours. This was followed by repeated sputtering (Ar^+, 1 kV) and annealing cycles, 5 min at 600 °C. The annealing temperatures were measured with infrared pyrometers.

Manganese was evaporated from a well-outgassed electron beam evaporator (Omicron/Focus) onto clean and well-ordered Ge(111)$c(2 \times 8)$ surfaces, at a rate of 0.5 ML/min, where 1 ML is defined as the number of the topmost atoms in the unreconstructed Ge(111) surface (1 ML = 7.21×10^{14} atoms/cm^2). The evaporator was carefully calibrated by a quartz crystal thickness monitor. The pressure during evaporation was lower than 1×10^{-10} mbar and $\sim 6 \times 10^{-11}$ mbar during measurements. After Mn deposition, a 6-ML sample was probed with STM and thereafter annealed at 330 °C for 20 min. After annealing, intense 1×1 diffraction spots as well as weak $c(2 \times 8)$ and threefold $\sqrt{3} \times \sqrt{3}$ spots were seen by LEED, in Fig. 1(a). Successive evaporations of 6-, 12-, and 8-ML Mn, formed surfaces with total coverages of 12-, 24-, and 32-ML Mn. Each surface was also annealed at 330 °C for 20 min [Figs. 1(b) and 1(c), respectively]. For a comparison, the 32-ML surface was further annealed at 450 °C [Fig. 1 (d)]. The resulting LEED patterns showed intense 1×1 and $\sqrt{3} \times \sqrt{3}$ diffraction spots. The photoemission experiment used samples prepared by the same method. In order to trace the detailed changes in the core levels, 3 ML was set up as an initial Mn coverage. To improve the spectral

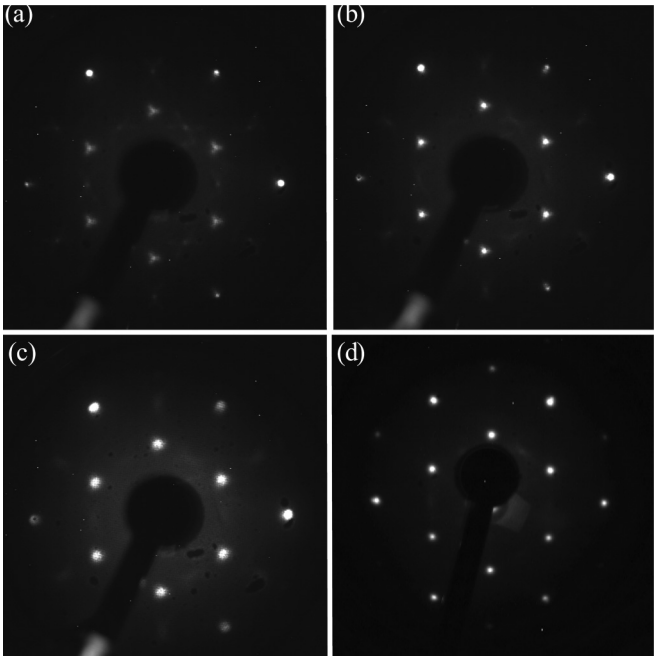

FIG. 1. LEED patterns from the Mn_5Ge_3 surfaces with different Mn coverages. (a)–(c) Annealed at 330 °C and (d) at 450 °C. (a) 6-ML sample showing a 1×1 and weak $c(2 \times 8)$ and $\sqrt{3} \times \sqrt{3}$ LEED diffraction spots. (b) 12-ML sample showing a $\sqrt{3} \times \sqrt{3}$ pattern. (c) 24-ML sample showing intense $\sqrt{3} \times \sqrt{3}$ pattern. (d) 32-ML sample showing intense $\sqrt{3} \times \sqrt{3}$ LEED pattern. Images (a)–(c) were recorded at 39 eV and (d) at 46 eV.

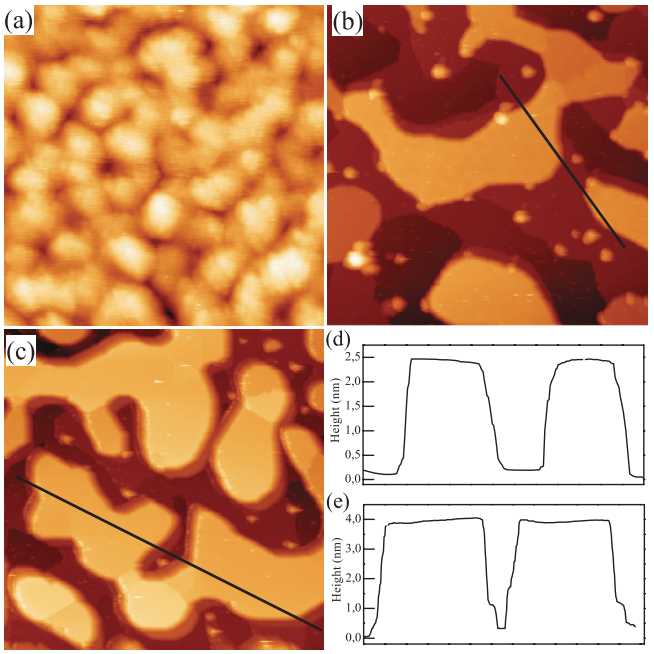

FIG. 2. (Color online) Topographic STM images from the Mn germanide surfaces. (a) 6-ML as-deposited sample recorded at $V_S = 2.35$ V, $I = 0.1$ nA, 40×40 nm. (b) 6-ML sample annealed at 330 °C showing large Mn_5Ge_3 islands, recorded at $V_S = 1.6$ V, $I = 10$ pA, 200×200 nm. (c) 12-ML sample after annealing at ~330 °C, $V_S = -1.6$ V, $I = 50$ pA, 300×300 nm. (d) Profile along the black line in (b) showing an average island height of 2.4 nm. (e) Profile along the black line in (c) showing an average height of 3.8 nm from the large islands in (c).

sharpness, the surfaces with higher Mn coverages were further cooled with liquid nitrogen (100 K).

III. RESULT AND DISCUSSION

Figures 2(a)–2(c) show topographic STM images from Mn germanide surfaces with 6-ML Mn. The 6-ML as-deposited sample [Fig. 2(a)] shows small manganese clusters uniformly distributed over the substrate with average diameters of 5 nm. Annealing of the as-deposited sample at 330 °C resulted in large flat islands with well-ordered surfaces, having a periodicity similar to the Ge(111)-($\sqrt{3} \times \sqrt{3}$). It is worth noting that the Mn_5Ge_3 1×1 unit cell has a similar lattice constant as the $\sqrt{3} \times \sqrt{3}$ surface of Ge(111). The Mn_5Ge_3 coverage is ~43% as estimated from the image-processing software.[15] The areas beside the islands show a $c(2 \times 8)$ surface reconstruction as expected from the LEED image [Fig. 1(a)]. The LEED image [Fig. 1(a)] did not show a simple $\sqrt{3}$ spot. Instead, a triple-split spot was observed. These can be explained by different domains in the Mn_5Ge_3 film structure with its unit vector slightly larger than the $\sqrt{3}$ vector.

In Fig. 2(c), a topographic STM image from the 12-ML Mn surface is shown. Large flat islands with a honeycomb surface structure on the top were formed. The coverage of the Mn_5Ge_3 phase is estimated to ~60%. Also, here the areas between the islands show the $c(2 \times 8)$ surface reconstruction. Figures 2(d) and 2(e) show line profiles along the black lines in Figs. 2(b) and 2(c), respectively. The average heights of the islands in the 6- and 12-ML surfaces are measured to be ~2.4 and ~3.8 nm. Figure 3(a) shows the 24-ML Mn surface after annealing. Compared to the 6-ML surface, even larger flat islands were formed with a honeycomb surface structure. The coverage of the Mn_5Ge_3 phase is estimated to ~73%. The height of the islands is ~6.5 nm, which is obtained from the line profile in Fig. 3(c) measured along the black line in Fig. 3(a).

Figure 3(b) shows the 32-ML sample after annealing at at 330 °C. Except for some small holes, the Ge substrate is almost fully covered by Mn_5Ge_3 film. This is similar to the MnSi growth,[16,17] which also shows holes in a fully grown film. In the case of MnSi, the holes were explained to act as a feedstock of Si for further MnSi growth. Possibly an alike situation also happens here. The 32-ML Mn film shows a honeycomb structure, which is similar to all other top surfaces of the islands for the 6-, 12-, and 24-ML surfaces. This observation is close to those reported in Refs. 4 and 10. Figure 3(d) shows a close-up image of such structure from Fig. 3(b). The white rhombus in Fig. 3(d) indicates the Mn_5Ge_3 surface unit cell. There are two white protrusions in each unit cell. As shown by the previous study, these protrusions most likely correspond to the top surface Mn atoms.[13] Besides, threefold point defects, seen in Fig. 3(d), were explained by missing atoms in the top structure of the film. The 32-ML sample was also annealed at 450 °C [Fig. 3(e)]. No obvious change in the surface morphology was found by STM, suggesting that the surface/film is very stable in the temperature range from 330–450 °C, in agreement with Ref. 1.

Based on the known structure of Mn_5Ge_3, the amount of evaporated Mn, and the measured surface area covered

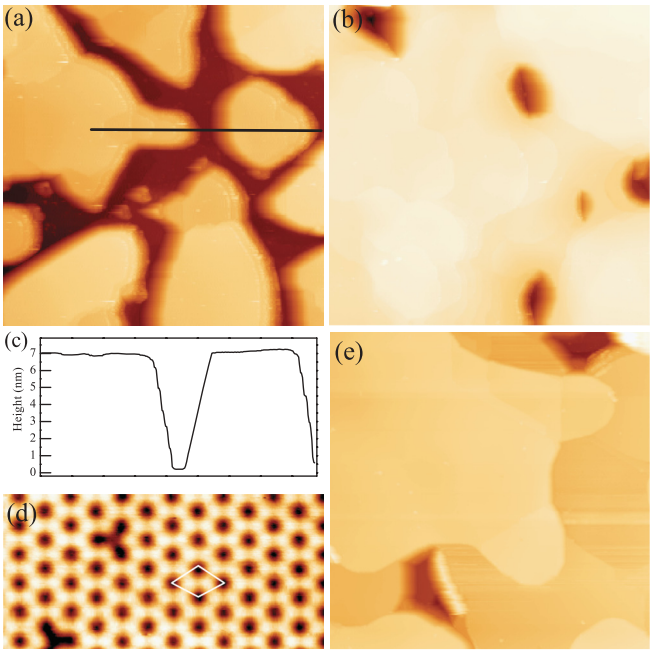

FIG. 3. (Color online) Topographic STM images from the Mn germanide surfaces annealed at 330°C [(a), (b), and (d)] and 450°C (e). (a) A 300 × 300 nm image from the annealed 24-ML sample, $V_S = -1.6$ V, $I = 50$ pA. (b) 300 × 300 nm image from the 32-ML sample annealed at 330°C, $V_S = -1.1$ V, $I = 50$ pA. (c) Line profile along the black line in (a) showing the height difference between the substrate and Mn_5Ge_3. (d) A 8 × 4 nm image from the 32-ML sample showing the honeycomb pattern, the white rhombus indicate the $\sqrt{3} \times \sqrt{3}$ unit cell, $V_S = -0.5$ V, $I = 25$ pA. (e) 300 × 300 nm image from the 32-ML sample, annealed at 450°C.

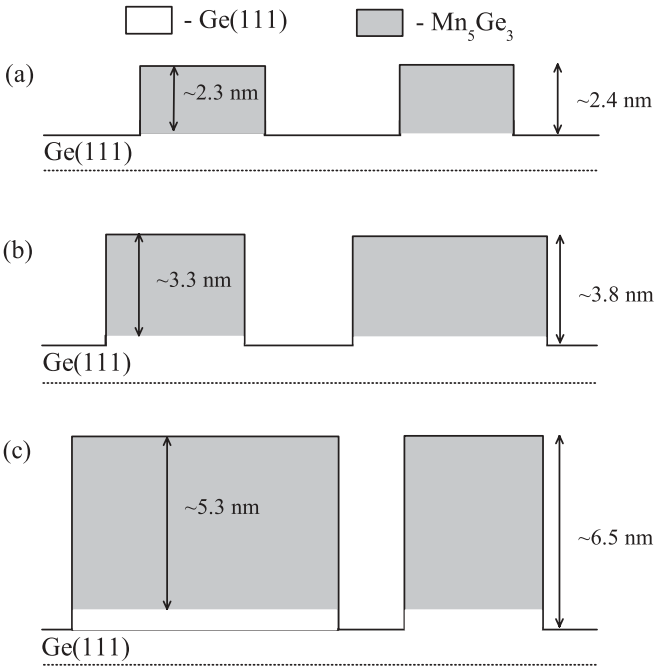

FIG. 4. Calculated and measured island heights for the 6-, 12-, and 24-ML Mn, (a)–(c), respectively. Gray areas are the calculated thicknesses of Mn_5Ge_3 based on the structure model. The total heights are measured from STM images.

by the islands, we can easily calculate the estimated height of the germanide islands. One layer of Mn_5Ge_3, 5 Å thick, can be made by evaporating 3.107-ML Mn. However, after evaporation of 6 ML Mn and annealing, the Mn migrated over the surface to form islands resulting in a Mn_5Ge_3 coverage of ~43%. By recalculating the same amount of Mn concentrated on the smaller surface area, one instead obtains an island height of 2.3 nm, which is close to the measured value of 2.4 nm. For 12- and 24-ML Mn, these give islands heights of 3.3 and 5.3 nm. This is in contrast to our STM measurements in which the island heights are 3.8 and 6.5 nm, respectively. Figure 4 illustrates the discrepancy between the calculated and measured island height.

These results give information about the growth mode for the formation of a Mn_5Ge_3 film. After deposition, the Mn are evenly distributed over the substrate. As illustrated in the previous figures, after annealing, the Mn have migrated over the surface to form islands, leaving a bare Ge(111)$c(2 \times 8)$ surface in-between the islands. Our results indicate that also a significant amount of Ge migrates from the bare areas to the islands, leaving the clean surface in a position lower than the Mn_5Ge_3/Ge(111) interface. With further Mn evaporation and annealing, the islands grow in height as well as in lateral directions, leaving deeper open areas in the film structure, with even larger differences between the calculated and measured island heights. It appears that the bare surfaces between the islands act as a Ge source during the germanide island growth. This growth procedure goes on until, finally, at 32 ML, the surface is almost fully covered (90%–95% coverage) by a Mn_5Ge_3 film, except for some holes in the film.

The core-level spectra reveal another important information on the Mn_5Ge_3 formation. Figure 5 shows an evolution of Ge 3*d* core levels with an increase of Mn coverages. In Fig. 5(a), the Ge 3*d* spectrum from the clean Ge(111)$c(2 \times 8)$ surface was recorded with a photon energy of 90 eV. The rest-atom state, marked A, and the bulk component (B) are clearly seen in the spectrum. With further Mn evaporations, the rest-atom state (A) decreases in intensity and is no longer visible at a coverage of 24 ML in Fig. 5(e). The Ge $3d_{3/2}$ bulk component ($B_{3/2}$), on the other hand, is still visible at 24 ML, but is no longer pronounced at 32 ML in Fig. 5(f). These observations are expected when comparing to the topographic STM images in Figs. 2 and 3, in which the germanide evolves from islands to an almost closed film. The development of new components (C_1, C_2, and C_3) is quite clear in Figs. 5(b)–5(f). These components first appear as broad features or small shoulders at low Mn coverages. With higher Mn coverages, the C_1 component appears as a clear shoulder and C_2 and C_3 as small peaks. It is obvious that at least two components develop with Mn evaporations and should be associated to Mn_5Ge_3.

Ge 3*d* spectra have also been studied at different photon energies in order to evaluate at which photon energy the Ge 3*d* core-level components from the Mn_5Ge_3 film are most resolved. The 24-ML sample is suitable for this purpose since it is still possible to trace the high-binding-energy shoulder that can be related to bulk Ge. Spectra (a)–(d) in Fig. 6 are recorded at photon energies of 50, 70, 90, and 110 eV, respectively. By following the evolution of the components with photon energies, it appears that C_1 and C_2 are mostly pronounced at

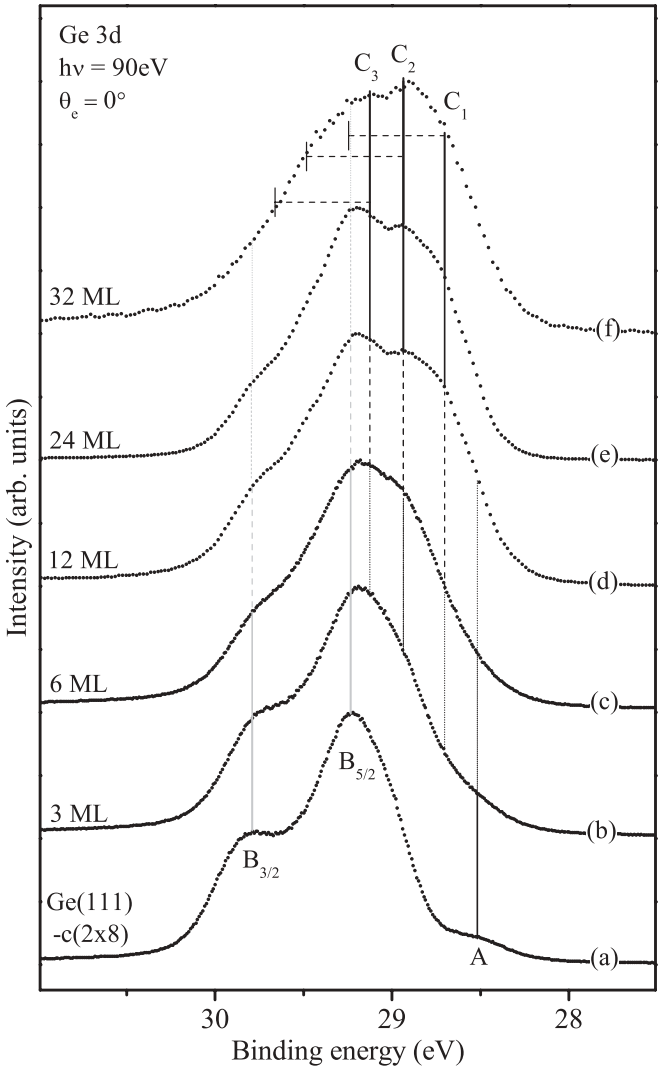

FIG. 5. High-resolution CLS spectra showing the evolution of Ge 3*d* core-level spectra with Mn coverages. Recorded at normal emission with incident angle 50° [(a)–(e)] and 45° (f) and 90-eV photon energy. Spectra (a)–(c) recorded at RT and (d)–(f) at 100 K.

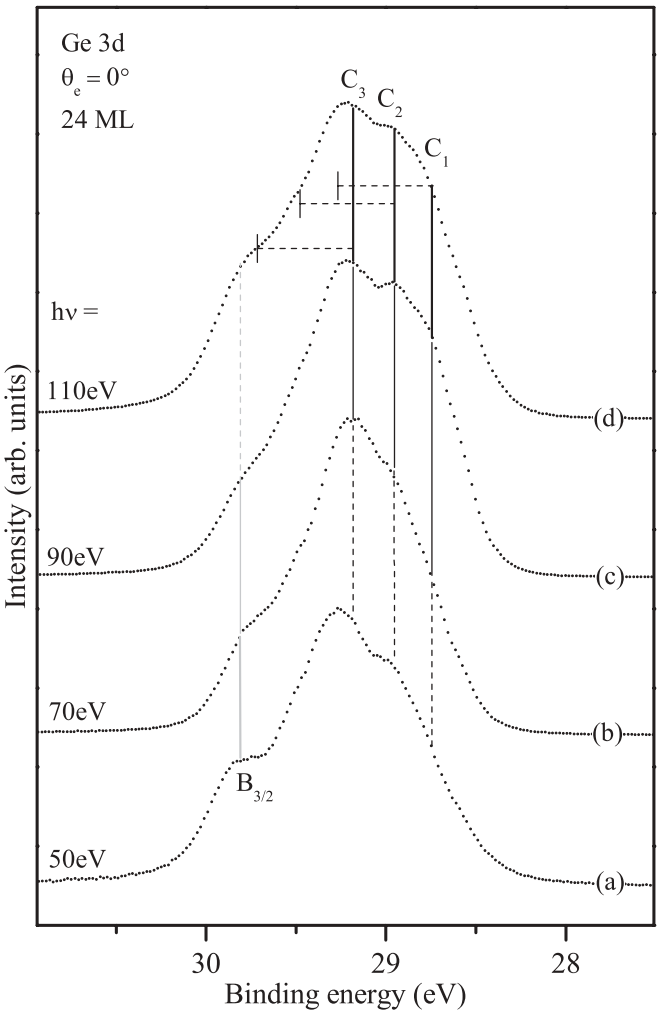

FIG. 6. High-resolution CLS spectra showing the evolution of Ge 3*d* core-level spectra with photon energies. Recorded at normal emission with incident angle 50°. Spectra (a)–(d) recorded at 100 K with photon energies 50, 70, 90, and 110 eV, respectively.

90 eV, while at 70 eV they are less intense. For a detailed core-level fitting, the Ge 3*d* spectra recorded at 70 and 90 eV have been chosen from the 32-ML sample and will be discussed below.

Figure 7 shows high-resolution Ge 3*d* spectra recorded at 100 K from the 32-ML Mn_5Ge_3 surface annealed at 450 °C. To achieve a consistent fit over the energy and angular range, a combined Shirley and parabolic background has been used.[18] In the fitting program,[19] Voigt line shapes were used with a Doniach-Šunjić singularity of $\alpha = 0.04$ for all spectra to take care of the metallic tails.[20] The spin-orbit split was held constant at 0.56 eV, Lorentzian width was set to 0.095 eV, and the Gausssian to 0.34 eV. The branching ratios were allowed to vary between 0.61 and 0.65 during the fitting procedure. The details about the line fit are listed in Table I. In Figs. 7(a)–7(d), the core-level spectra were recorded with photon energies of 70 and 90 eV at 0° and 60° emission angles. Three components are needed to fit these spectra in a satisfactory way. Two components, C_1 and C_2, are visible as peaks or shoulders in the raw spectra in Figs. 7(a)–7(d). To achieve a consistent fit over the energy and angular range one more component, C_3, has to be introduced in the line profile analysis. Compared to the bulk component from the clean Ge(111)$c(2 \times 8)$, C_1, C_2, and C_3 are shifted towards lower binding energy by −0.62, −0.35, and −0.055 eV, respectively.

The Ge 3*d* spectrum, recorded with 90-eV photon energy in Fig. 7(c), is more surface sensitive than the spectrum in Fig. 7(a) since in this energy range, the mean-free path of the electrons decreases with increasing kinetic energy.[21,22] In Figs. 7(a) and 7(c), the C_1 component increases in intensity with surface sensitivity. Also, in the enhanced surface-sensitive spectrum recorded at 60° emission angle [Fig. 7(b)], this component becomes more intense compared to the bulk sensitive spectrum [Fig. 7(a)]. These facts together with the relative intensities in Table I show that C_1 is a surface-related component.

The C_2 component is the most intense component. In the spectra recorded at photon energies of 70 and 90 eV and 60° emission angle [Figs. 7(a)–7(d)], C_2 almost has a constant intensity. As shown in Fig. 5, C_2 grows hand in hand with

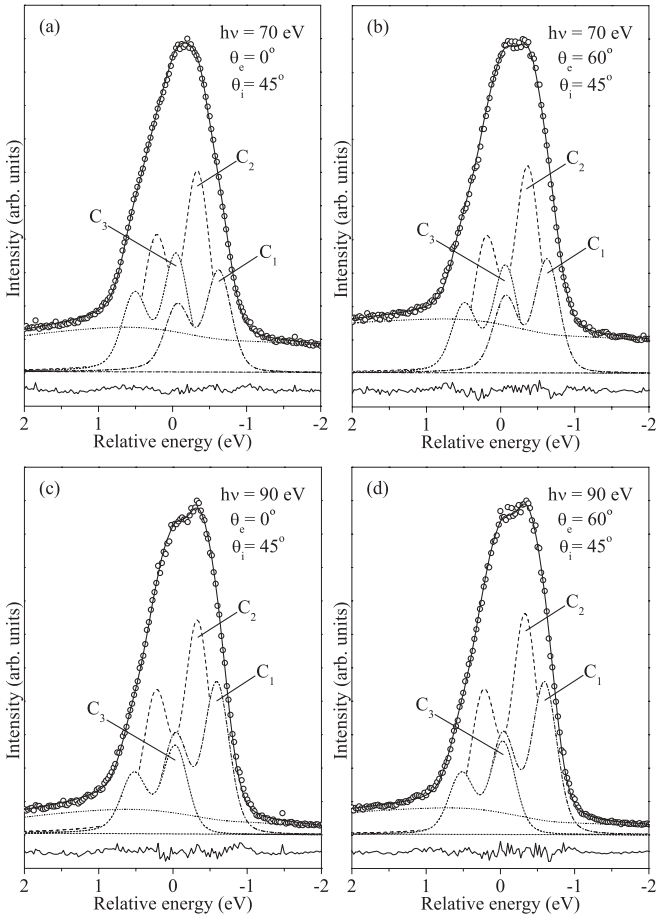

FIG. 7. High-resolution Ge 3*d* core-level spectra recorded at 100 K: [(a) and (c)] normal emission, and [(b) and (d)] 60° emission. All the incident angles were 45°. The spectra were recorded with photon energies of 70 and 90 eV. The solid lines show the total contribution from the components used to fit the experimental data (circles). Underneath each spectrum, the residual lines from the fitting procedure are presented.

increasing Mn coverages. The total impression indicates that C_2 is a component clearly related to the Mn_5Ge_3 film. C_3 is more pronounced in the bulk sensitive spectrum recorded with 70 eV at normal emission. With higher photon energy and emission angle, C_3 becomes less intense. This indicates that C_3 has a more bulklike character.

In order to explain the line profiles, we have compared our results to an atomic model of the Mn_5Ge_3 germanide, drawn in Fig. 8 (according to Ref. 12).[12,13] The unit cell of Mn_5Ge_3 along the [001] crystallographic direction possesses four atomic layers stacked along the z direction. Two layers containing only Mn atoms and labeled Mn_I are located at $z = 0$ and $1/2$. The other two layers contain an equal amount of Mn (Mn_{II}) and Ge atoms and are located at $z = 1/4$ and $3/4$. In this case, there are two possible surface terminations: only a Mn layer or a mixed Mn/Ge layer. Earlier reports regarding the surface termination of Mn_5Ge_3 suggested that the surface is terminated by Mn atoms (Mn_I).[2–5,17]

From the line-shape analysis, one finds that C_1 is the most surface-sensitive component (see Table I). Compared to the model in Figs. 8(a) and 8(b), the most surface-related Ge

TABLE I. Parameter details used to fit the spectra in Figs. 7(a)–7(d). In all spectra, the Lorentzian and Guassian full widths at half maximum (FWHMs) were kept constant at 0.095 and 0.34 eV, respectively. The spin-orbit splitting was held constant at 0.56 eV and the branching ratios were allowed to vary between 0.61 and 0.65. A singularity index of $\alpha = 0.04$ has been used in all the spectra. Peak intensity variations are shown in percent (%) of the total intensity. BE denotes binding energy.

		Intensity(%)			
	Relative BE	70 eV		90 eV	
Component	(eV)	0°	60°	0°	60°
C_1	−0.62	24.0	26.6	33.2	32.6
C_2	−0.35	48.0	48.5	47.0	47.4
C_3	−0.055	28.0	24.9	19.8	20.0

exists in the first mixed Mn/Ge layer. These Ge atoms may receive extra charge from the top-most Mn, resulting in a large core-level shift. Thus, C_1 may originate from the first mixed Mn/Ge layer. The C_2 component is not changing with different photon energies and emission angles. However, as mentioned above, its intensity increases with increasing Mn coverages, indicating that C_2 belongs to the Mn germanide. Due to the high intensity and surface sensitivity, this component is considered to originate from the Ge in the MnGe film, e.g., the second and lower-lying mixed Mn/Ge layers.

The third component C_3, which decreases in intensity with increased photon energies and emission angles, has a more bulklike character. As illustrated in Fig. 6, this component has a binding energy close to the bulk component of the clean Ge(111)$c(2 \times 8)$ spectrum. However, this component should not be a pure Ge bulk component since from STM one expects no more than ∼10% contribution for a bulk component (from the holes in the film structure). To conclude this part, we tentatively assign C_3 as deep-lying mixed Mn/Ge layers, plus a pure Ge bulk contribution.

To further understand the electronic structure of the Mn_5Ge_3 film, Mn 2*p* spectra have also been investigated. All annealed Mn 2*p* spectra show clear similarity, irrespective of the Mn coverages. Figure 9 shows the Mn 2*p* CLS spectra recorded from the 3-ML as-deposited and annealed 24-ML samples. The as-deposited spectrum is presented for comparison and shows a spin-orbit split of 11.25 eV. This

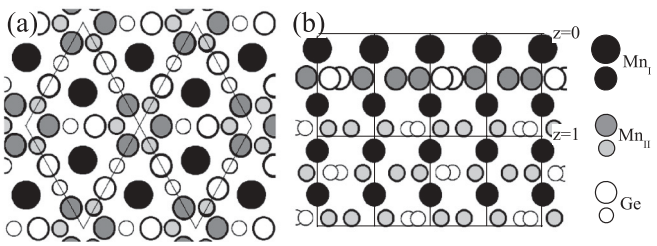

FIG. 8. Atomic model of Mn_5Ge_3 exposed (0001) plane. (a) Top view with the $\sqrt{3} \times \sqrt{3}$ unit cells indicated by the black line. (b) Side view of the germanide structure in (a). Black large spheres represent Mn_I atoms in the top layer and Mn-only layers. Dark gray and light gray spheres represent Mn_{II} atoms in the first and deeper-lying mixed Mn/Ge layers, respectively. White spheres represent Ge atoms.

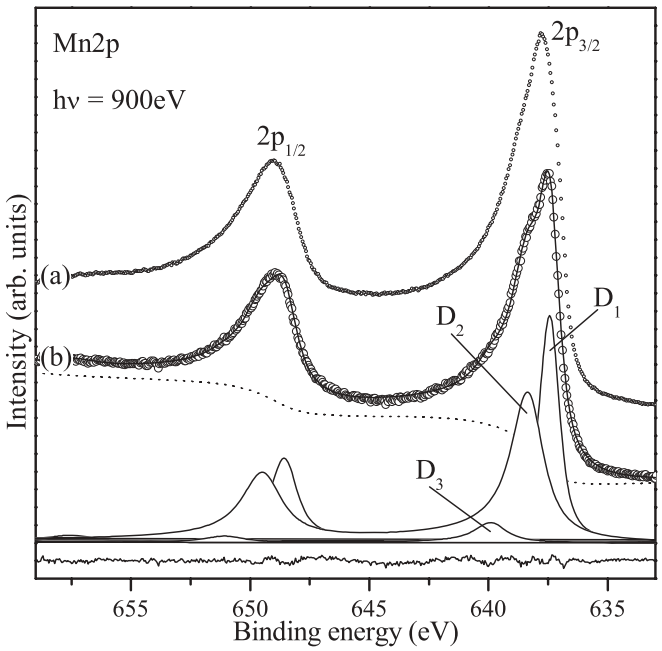

FIG. 9. Mn $2p$ spectra recorded with 900-eV photon energy. (a) As-deposited 3 ML at RT. (b) 24-ML annealed sample at LN temperature. The solid lines show the total contribution from the components used to fit the experimental data (circles). Underneath the spectra, the residual line from the fitting procedure is presented.

value is in agreement with a thick Mn layer deposited on a metal surface,[23] and thus may be regarded as a reference for bulk Mn.

For the annealed 24-ML sample, a consistent fitting was done using Voigt line shapes with a Doniach-Šunjić singularity $\alpha = 0.08$. To take into account for the Coster-Kronig broadening, the Lorentzian widths for the $2p_{1/2}$ components were set broader than those for the $2p_{3/2}$ ones.[24–26] The spin-orbit splitting of the main components is 11.43 eV, which is close to the calculated value (11.4 eV) for a monovalent ($3d^6$) Mn ion in spherical symmetry.[27] The details about the fitting are listed in Table II. The main sharp component (D_1) is located at a binding energy of 637.4 eV. Besides, there is a clear shoulder peak D_2 shifted by ~0.91 eV towards higher binding energy. This spectrum is similar to the one recorded from the Mn_5Si_3 film in Ref. 28, where the shift of the shoulder peak is only 0.66 eV.

A third component (D_3) that is needed to achieve a consistent fit is shifted by ~2.46 eV towards higher binding energy. We tentatively assign this component as a satellite peak

TABLE II. Parameter details used to fit the spectra in Fig. 9. In all spectra, the Guassian FWHMs were kept constant at 0.51 eV. In the Mn $2p$ spectrum, the spin-orbit splitting was 11.14 eV. BE and BR denote binding energy and branching ratio, respectively.

	Component	Relative BE	$L_{3/2}$	$L_{1/2}$	BR	α
Mn $2p$	D_1	0	0.65	1.06	0.51	0.08
	D_2	0.905	1.35	1.76	0.54	0.08
	D_3	2.46	1.35	1.76	0.40	0.08

due to fine features from various Mn atomic configurations.[29] D_1 has a narrower line profile compared to D_2 and D_3. In a line-shape analysis, this is often the case for a bulk-related component and D_1 can therefore be regarded as originating from the bulk Mn_5Ge_3 film. In earlier studies, D_2 was interpreted as a satellite structure component related to the interaction between the Mn $2p_{3/2}$ core hole and the partially filled $3d^n$ shell.[23,30] In our case, D_2 can be consistently fitted in both the $2p_{1/2}$ and $2p_{3/2}$ peaks. On the other hand, the D_2 component has an opposite core-level shift compared to the Ge $3d$ ones. One therefore may interpret D_2 as a surface component due to a net charge transfer from Mn to Ge. However, the D_2 component has a much broader line profile compared to D_1 and might also contain a contribution related to the Mn $2p$-$3d$ exchange interaction.

In earlier photoemission studies, Sangaletti *et al.*[6] only used one component, except for the bulk one, to fit a Ge $3d$ spectrum from a similar Mn_5Ge_3 $\sqrt{3} \times \sqrt{3}$ surface. This component was shifted by 0.53 eV to lower binding energy compared to the bulk peak. It was then assigned to Ge atoms surrounded by Mn atoms in an alloylike environment. De Padova *et al.*[7] used one D-S doublet shifted 0.426 eV toward lower binding energy. In their fitting, they used different values of the Lorentzian FWHM for the Ge $3d_{5/2}$ (76 meV) and Ge $3d_{3/2}$ (91 meV) components. This was explained as a consequence of the M_4-M_5V Coster-Kronig transition. In our fitting procedure, we obtained a worse fit using different values for the Lorentzians and instead three peaks have been found, i.e., two surface-sensitive peaks (C_1 and C_2) and one peak (C_3) with a bulklike character. Compared to one big Mn_5Ge_3 component in Refs. 6 and 29, the C_1 and C_2 components, shifted to lower binding energies, find a natural explanation in the layered structure of Mn_5Ge_3. It is plausible to expect that the top Ge in the $\sqrt{3} \times \sqrt{3}$ reconstruction has a different core-level shift compared to deeper-lying Ge in the film. As in the MnSi case in Ref. 31, two components were used to explain the film structure, i.e., one component for the top Si terminating the surface and one for deeper-lying Si in the film. This is also consistent with the Mn $2p$ spectra that have an opposite core-level shift compared to the Ge $3d$ spectra. We note that in Refs. 6 and 7, there are no reports of island formation. On the contrary, de Padova *et al.* (Ref. 7) report a continuous germanide film that is strained. This is clearly different from our results at similar coverages. The strong tendency to form islands reported here for the annealing temperatures 330°C and 450°C imply that we have instead formed a relaxed Mn_5Ge_3 layer. This may be one reason for the differences in the Ge $3d$ core-level data.

IV. CONCLUSIONS

In conclusion, the morphology and electronic structure of Mn_5Ge_3 have been investigated by STM and CLS. A fully covered Mn_5Ge_3 film was formed at 32-ML Mn coverage after 330°C annealing. We have observed a growth mode for the formation of a Mn_5Ge_3 film on Ge(111)$c(2 \times 8)$ involving island formation with a significant surface diffusion. In comparison to earlier results, a more detailed analysis of the Ge $3d$ core-level spectra has been presented here. Three components are needed for a consistent fitting of

the Ge 3*d* core-level spectra on the Mn_5Ge_3 surface. In addition, three components have been identified for the Mn 2*p* core-level spectra. The two major components fit well with the established layered Mn_5Ge_3 structural model found in the literature.

ACKNOWLEDGMENTS

The authors would like to thank the Swedish National Graduate School in Materials Science and the MAX-lab staff. This work was supported by the Swedish Research Council.

*Joakim.Hirvonen@kau.se

[1] C. Zeng, S. C. Erwin, L. C. Feldman, A. P. Li, R. Jin, Y. Song, J. R. Thompson, and H. H. Weitering, Appl. Phys. Lett. **83**, 5002 (2003).

[2] L. J. Chen, D. Y. Wang, Q. F. Zhan, W. He, Q. A. Li, and Z. H. Cheng, Chin. Phys. B **17**, 3902 (2008).

[3] S. A. Wolf, D. D. Awschalom, R. A. Buhrman, J. M. Daughton, S. von Molnar, M. L. Roukes, A. Y. Chtchelkanova, and D. M. Treger, Science **294**, 1488 (2001).

[4] C. Zeng, W. Zhu, S. C. Erwin, Z. Zhang, and H. H. Weitering, Phys. Rev. B **70**, 205340 (2004).

[5] L. Sangaletti, D. Ghidoni, S. Pagliara, A. Goldoni, A. Morgante, L. Floreano, A. Cossaro, M. C. Mozzati, and C. B. Azzoni, Phys. Rev. B **72**, 035434 (2005).

[6] L. Sangaletti, E. Magnano, F. Bondino, C. Cepek, A. Sepe, and A. Goldoni, Phys. Rev. B **75**, 153311 (2007).

[7] P. De Padova, J.-M. Mariot, L. Favre, I. Berbezier, B. Olivieri, P. Perfetti, C. Quaresima, C. Ottaviani, A. Taleb-Ibrahimi, P. Le Fèvre, F. Bertran, O. Heckmann, M. C. Richter, W. Ndiaye, F. D'Orazio, F. Lucari, C. M. Cacho, and K. Hricovini, Surf. Sci. **605**, 638 (2011).

[8] A. Verdini, A. Cossaro, L. Floreano, A. Morgante, A. Goldoni, A. Sepe, S. Pagliara, and L. Sangaletti, Surf. Sci. **600**, 4369 (2006).

[9] A. Verdini, A. Cossaro, L. Floreano, A. Morgante, A. Goldoni, D. Ghidoni, A. Sepe, S. Pagliara, and L. Sangaletti, Phys. Rev. B **77**, 075405 (2008).

[10] H. Kim, G.-E. Jung, J. K. Yoon, K. H. Chung, and S.-J. Kahng, Surf. Sci. **602**, 481 (2008).

[11] H. Kim, G.-E. Jung, J.-H. Lim, K. H. Chung, S.-J. Kahng, W.-J. Son, and S. Han, Nanotechnology **19**, 025707 (2008).

[12] J. B. Forsyth and P. J. Brown, J. Phys.: Condens. Matter **2**, 2713 (1990).

[13] J. H. Grytzelius, H. M. Zhang, and L. S. O. Johansson, Phys. Rev. B **84**, 195306 (2011).

[14] B. N. Jensen, S. M. Butorin, T. Kaurila, R. Nyholm, and L. I. Johansson, Nucl. Instrum. Methods A **394**, 243 (1997).

[15] I. Horcas, R. Fernández, J. M. Gómez-Rodríguez, J. Colchero, J. Gómez-Herrero, and A. M. Baro, Rev. Sci. Instrum. **78**, 013705 (2007).

[16] A. Kumar, M. Tallarida, M. Hansmann, U. Starke, and K. Horn, J. Phys. D: Appl. Phys. **37**, 1083 (2004).

[17] J. Hirvonen Grytzelius, H. M. Zhang, and L. S. O. Johansson, Phys. Rev. B **80**, 235324 (2009).

[18] D. A. Shirley, Phys. Rev. B **5**, 4709 (1972).

[19] D. L. Adams and J. N. Andersen, FitXPS Version 2.12, http://www.sljus.lu.se/download.html.

[20] S. Doniach and M. Šunjić, J. Phys. C: Solid State Phys. **3**, 285 (1970).

[21] C. J. Karlsson, E. Landemark, Y.-C. Chao, and R. I. G. Uhrberg, Phys. Rev. B **50**, 5767 (1994).

[22] J. J. Paggel, W. Thesis, K. Horn, Ch. Jung, C. Hellwig, and H. Petersen, Phys. Rev. B **50**, 18686 (1994).

[23] A. K. Shukla, P. Krüger, R. S. Dhaka, D. I. Sayago, K. Horn, and S. R. Barman, Phys. Rev. B **75**, 235419 (2007).

[24] R. Nyholm, N. Mårtensson, A. Lebugle, and U. Axelsson, J. Phys. F: Metal Phys. **11**, 1727 (1981).

[25] A. Cheng, M. L. Klein, and L. J. Lewis, Phys. Rev. B **44**, 13 (1991).

[26] M. Ohno and G. A. van Riessen, J. Electron Spectrosc. Relat. Phenom. **128**, 1 (2003).

[27] P. Krüger and A. Kotani, Phys. Rev. B **68**, 035407 (2003).

[28] A. Irizawa, A. Yamasaki, M. Okazaki, S. Kasai, A. Sekiyama, S. Imada, S. Suga, E. Kulatov, H. Ohta, and T. Nanba, Solid State Commun. **124**, 1 (2002).

[29] L. Sangaletti, G. Drera, E. Magnano, F. Bondino, C. Cepek, A. Sepe, and A. Goldoni, Phys. Rev. B **81**, 085204 (2010).

[30] A. Gloskovskii, G. Stryganyuk, G. H. Fecher, C. Felser, S. Thiess, H. Schultz-Ritter, W. Drube, G. Berner, M. Sing, R. Claessen, and M. Yamamoto, J. Electron Spectrosc. Relat. Phenom. **185**, 47 (2012).

[31] J. Hirvonen Grytzelius, H. M. Zhang, and L. S. O. Johansson, Phys. Rev. B **78**, 155406 (2008).